# Leading Edge of a Hydraulic Fracture Crossing a Stress Boundary

D. I. Garagash[1], A. Rohde[2], and A. P. Bunger[2]
[1] *Dept. of Civil and Resource Engineering, Dalhousie University, Halifax, Canada*
[2] *CSIRO Division of Petroleum Resources, Melbourne, Australia*

ABSTRACT

The presence of stress and material interfaces in hydrocarbon reservoirs may significantly complicate prediction of hydraulic fracture propagation, as the spatial resolution of numerical codes is usually insufficient to capture the details of the fracture-interface interaction at the early stages of the crossing. Thus, an explicit analytical and experimental investigation of the leading edge of the fracture normally crossing a stress interface (where the stress component normal to the fracture plane is discontinuous) is undertaken under conditions when solid toughness, fluid leak-off, and fluid lag are negligible. The analytical plane strain solution corresponds to that of a semi-infinite hydraulic fracture, which propagation velocity varies with the penetration depth past the interface. When appropriately scaled, the solution depends on a single dimensionless penetration depth parameter or time. Comparison with the experimental results for initially penny-shape hydraulic fractures crossing a stress interface in PMMA shows remarkable agreement in a wide range of penetration values.

## 1 INTRODUCTION

Numerical modelling of a hydraulic fracture as it grows past a sudden jump in the in situ stress field and/or material properties requires the leading edge to be appropriately resolved on a lengthscale which is typically much smaller that the desired spatial resolution of a numerical method. One possible approach to overcome this difficulty relies on enriching the numerical algorithm with a "tip logic," which means that the correct leading edge ('tip') asymptotic solution in the immediate vicinity of a stress boundary is embedded in the numerical algorithm. The tip solution considered in this paper depends only on the *local values* (near the fracture front) of the material and fracture properties, such as the rock and fluid properties, the magnitude and the sign of the stress jump, the penetration past the interface, and the velocity of the fluid flowing into the tip region [1, 2]. The latter acts as a parameter that couples the tip solution to the overall fracture solution. The tip solution, provided in this paper under conditions of zero fracture toughness, zero fluid leak-off, and zero fluid lag, is compared, and shown to be in good agreement with the results of zero-toughness, laboratory scale hydraulic fracturing experiments.

## 2 TIP SOLUTION

### *2.1 Model Formulation*

Consider a semi-infinite fluid-driven fracture propagating under a plane strain condition at initially constant velocity $V_o$ in the direction of the fixed coordinate axis

$X$, see Fig. 1. The fracture propagates in the plane perpendicular to the minimum in-situ confining stress, which magnitude $\sigma(X) = \sigma_o \pm \Delta\sigma H(X)$ (where $H(X)$ is the Heaviside step function) changes step-wise at the interface $X = 0$ from $\sigma_o$ to $\sigma_1 = \sigma_o \pm \Delta\sigma$. Here $\Delta\sigma$ is the magnitude of the stress jump, while the sign corresponds to the sense of the jump ('+' corresponds to a positive jump, or stress increase in the direction of the crack propagation; and '−' corresponds to a negative jump, or stress decrease in the direction of crack propagation). Upon the moment when the fracture tip reaches (and crosses) the stress interface $X_{tip} \geq 0$, the fracture tip velocity $V$ is expected to deviate from its initially constant value $V_o$ with increasing penetration depth $\lambda = X_{tip} \geq 0$.

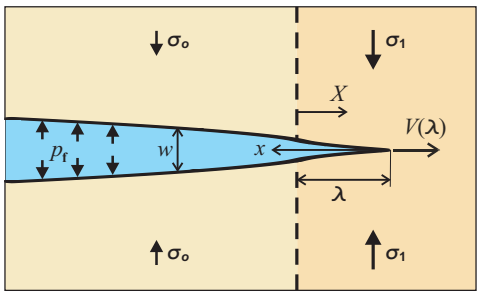


Figure 1: Hydraulic fracture tip crossing a stress interface.

Propagation of the semi-infinite fluid-driven fracture across a stress interface is considered under the following assumptions of: (i) unidirectional lubrication flow of incompressible Newtonian fluid in the crack; (ii) zero fluid leak-off (e.g., impermeable solid); (iii) linear elastic solid with zero toughness (e.g., fracture propagates along preexisting weakness plane or discontinuity); (iv) homogeneous solid properties and perfectly-bonded stress interface (i.e., no opening or shearing of the physical interface corresponding to mathematical stress jump in response to the crossing fracture is allowed); and (v) fluid front coincides with the fracture tip (i.e., zero fluid lag).

Under the above assumptions, the solution for the crack opening $w$, fluid pressure $p_f$, and crack tip penetration depth $\lambda$ as a function of time $t$ ($t = 0$ when $\lambda = 0$) and distance from the crack tip $x = X_{tip} - X > 0$ ($w$ and $p_f$ only) is governed by the following equations.

The fluid flow in the fracture is governed by lubrication equations (local fluid mass balance and Poiseuille's law) written in the coordinate system ($x$) moving with crack tip

$$\frac{\partial w}{\partial t} + V\frac{\partial w}{\partial x} = \frac{\partial wv}{\partial x} \quad \left(V = \frac{\mathrm{d}\lambda}{\mathrm{d}t}\right), \qquad v = \frac{w^2}{\mu'}\frac{\partial p_f}{\partial x}, \tag{1}$$

respectively. Here $\mu' = 12\mu$ is a multiple of dynamic fluid viscosity $\mu$.

Opening of the crack faces $w$ is related to the applied net loading $p_f - \sigma$ via [3]

$$w(x,t) = 4\left(\frac{2}{\pi}\right)^{1/2} K_I\sqrt{x} + \frac{4}{\pi}\int_0^\infty K\left(\frac{s}{x}\right)\frac{p_f(s,t)-\sigma\left(s-\lambda(t)\right)}{E'}\mathrm{d}s, \tag{2}$$

where $E'$ is the plane strain solid modulus and the integral kernel is defined as $K(z) = \ln(|1+\sqrt{z}|\,/\,|1-\sqrt{z}|) - 2/\sqrt{z}$. The crack tip stress intensity factor $K_I$ in (2) is zero, $K_I = 0$, under the assumed condition of zero solid toughness,

### *2.2 Solution*

The structure of the solution can be understood by considering the near ($x \to 0$) and the far ($x \to \infty$) field asymptotics of a semi-infinite fluid-driven crack under the previously stated assumptions (e.g., [3, 2, 1]). Since the near or far fields are characterized by distances from the tip either much smaller or much larger then the distance to the stress interface, respectively, it is expected that the solution there is dominated by the locally homogeneous stress field(s). The corresponding asymptotics can be written in the form

$$w = \beta_o L_m^{1/3}(v)\, x^{2/3}, \qquad \frac{p_f-\sigma}{E'} = \delta_o L_m^{1/3}(v)\, x^{-1/3} \tag{3}$$

where the fluid velocity $v$ takes on the value of the instantaneous crack tip velocity $V(t)$ in the near field and a value $V_o$ in the far field:

$$\begin{array}{lll} x \to 0: & v = V(t), & \sigma = \sigma_o \pm \Delta\sigma\, H(\lambda(t)) \\ x \to \infty: & v = V_o & \sigma = \sigma_o \end{array} \tag{4}$$

In (3), $\beta_o = 2^{1/3}3^{5/6}$, $\delta_o = -6^{-2/3}$, and $L_m(v)$ is a characteristic lengthscale of viscosity processes defined as a product of fluid velocity $v$ on a characteristic timescale $T_m$ as follows

$$L_m(v) = v\,T_m, \qquad T_m = \frac{\mu'}{E'}. \tag{5}$$

To justify (3), consider crack propagation prior to the crossing ($\lambda(t) \le 0$) when the solution is independent from the distance to the interface and, therefore, corresponds to that of a semi-infinite crack steadily propagating in the homogeneous stress field $\sigma_o$. The solution [4, 5, 6] for this case is characterized by the uniform fluid velocity along the crack, $v(x) = V_o$, and is given by (3) everywhere along the crack (not just in the near or far fields). The non-LEFM form of the crack opening in (3), $w \sim x^{2/3}$ and corresponding negative net pressure singularity, $p \sim -x^{-1/3}$ are the consequence of the coupling between the lubrication fluid flow and the elastic crack deformation in the tip region under conditions of zero lag and *zero fracture toughness*. The latter implies negligible energy release rate at the crack tip as compared to the energy dissipation in the viscous fluid flow along the crack [1, 2, 3]. The perturbation introduced into the solution near the tip once it crosses the interface ($\lambda(t) > 0$) does not change the far field fluid velocity (away from this perturbation), which, therefore, remains equal to the constant $V_o$ at all times.

In view of the above, the solution after the crossing ($\lambda(t) > 0$) is sought as a time-dependent transition between the near and far fields given by (3-5). The numerical method is based on the extension of the approach originally developed for the solution of steady semi-infinite crack propagation [3, 2], where the extension allows the method to handle time-dependent propagation. The original approach relies on definition of a computational interval $x \in (x_0, x_\infty)$ such that the solution outside of this interval is approximated by the respective (near or far field) asymptote. Net pressure is then approximated by a piecewise constant function over a discretized computational interval. Using the net-pressure approximation, the elasticity integral (2) for the crack opening is then evaluated exactly. The resulting net-pressure and opening approximations are used with a finite-difference approximation of the lubrication equations (1) to provide a system of ordinary differential equations to be solved for the time evolution of the net-pressure at the discretization grid points, and of the penetration depth. Complete details of the solution are to be published elsewhere [1].

In solving this problem, it is important to acknowledge that the solution posses a universal scaling [1]

$$\begin{aligned} &\lambda(t) = L(V_o)\,\Lambda\left(\tfrac{t}{T}\right), \qquad V(t) = V_o\,\mathscr{V}\left(\tfrac{t}{T}\right), \\ &w(x,t) = \varepsilon\, L(V_o)\,\mathscr{W}\left(\tfrac{x}{L(V_o)}, \tfrac{t}{T}\right), \qquad p(x,t) - \sigma_o = \Delta\sigma\,\mathscr{P}\left(\tfrac{x}{L(V_o)}, \tfrac{t}{T}\right) \end{aligned} \tag{6}$$

where small number $\varepsilon$, lengthscale $L(v)$ and timescale $T$ are defined as follows

$$\varepsilon = \frac{\Delta\sigma}{E'}, \qquad L(V) = V\,T, \qquad T = \frac{T_m}{\varepsilon^3} = \frac{\mu' E'^2}{\Delta\sigma^3}. \tag{7}$$

This scaling (6) means that the positive and negative stress jump cases each can be described by one universal solution for the normalized penetration $\Lambda$, crack tip velocity $\mathscr{V}$, crack opening $\mathscr{W}$ and the net-pressure $\mathscr{P}$ as functions of normalized time $t/T$ and distance from the tip $x/L(V_o)$. The basic character of these tip solutions is discussed later, in the context of the comparison to the results of the experimental program, as described next.

## 3 EXPERIMENTAL PROCEDURE

A sketch of the experimental system used to monitor fluid-driven fracture growth through stress interfaces is shown in Fig. 2. The experimental method makes use of hydraulic fracture growth along the unbonded interface between two 355 x 400 x 175 mm PMMA blocks stacked one on top of the other. A 50 mm wide strip region of lower stress has been created along the interface by machining the contact surfaces of one of the blocks according to the Flamant solution, e.g., [7],

$$u_z = -a\frac{\Delta\sigma}{\pi E'}\left(\left(1+\frac{x}{a}\right)\ln\left(1+\frac{x}{a}\right)^2 + \left(1-\frac{x}{a}\right)\ln\left(1-\frac{x}{a}\right)^2\right) + C$$

where $u_z$ is the machining depth at location $x$, $\Delta\sigma = 4.3$ MPa is the desired stress contrast and $2a = 50$ mm is the strip width [8]. The arbitrary constant C is chosen

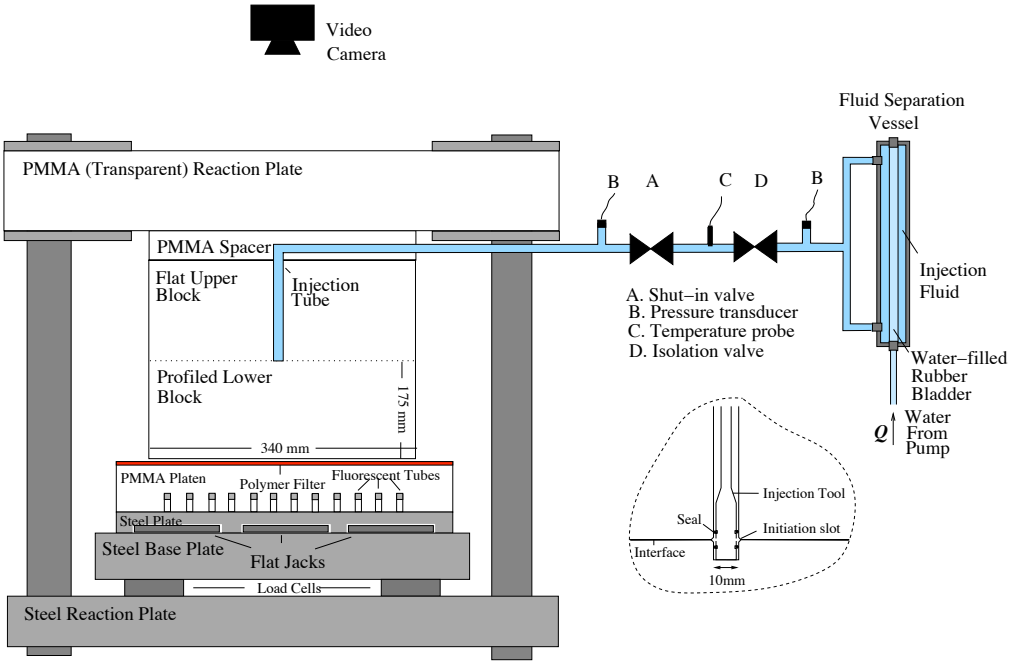


Figure 2: Sketch of the experimental system. The inset shows the details of the bottom-hole injection assembly.

here so that the displacement at the edge of the block is zero. Additionally, the plane strain modulus $E' = 3930$ MPa is the elastic property of the PMMA material as determined by uniaxial compression testing of a cylindrical strain-gauged specimen.

The blocks were uniaxially loaded using water-filled stainless steel flat jacks in a reaction frame that has been specially modified to allow viewing of the specimen during the experiment. The total applied vertical load was measured using four load cells located beneath the PMMA base platen. Fluid was injected into the interface via a 5 mm radius borehole located in the low stress region for the positive stress jump experiments, Fig. 3a, and in the high stress region for the negative stress jump experiments, Fig. 3b, using the constant displacement pump and a small straddle packer system to isolate a 5 mm long interval across the interface (Fig.2, inset). The initially penny-shape fractures loose their symmetry once the stress interface is reached by the fracture leading edge, developing the asymmetric foot print qualitatively shown on Fig. 3(a-b) with the continual propagation biased in the low stress region.

The growing fracture was monitored using a Canon XM2 digital video camcorder and a backlight that is built into the steel base plate. The recordings are used to monitor the location of the crack front and to produce an approximation of the light intensity profile resulting from the presence of colored fracture fluid being injected into the interface. The full-field fracture opening width is recovered from these

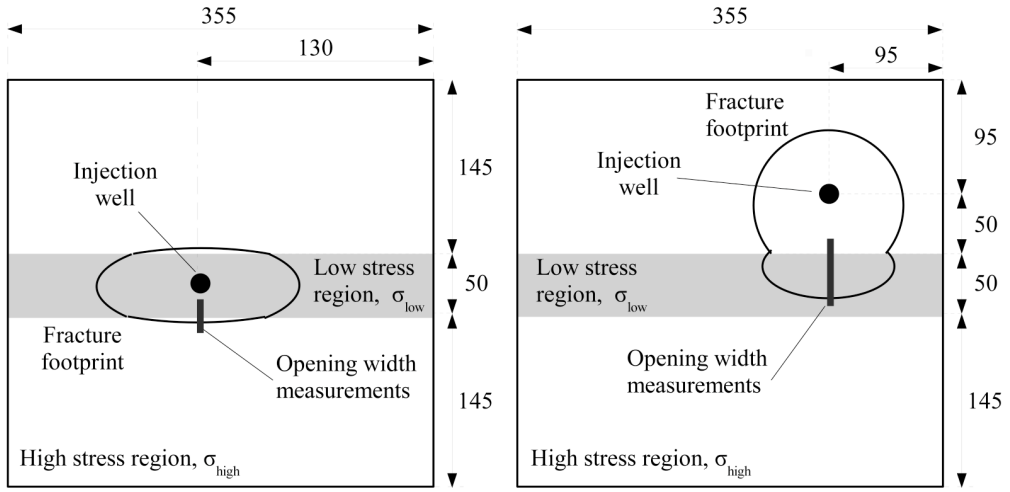


Figure 3: Stress and injection configuration for (a) positive stress jump and (b) negative stress jump experiments. Thick lines indicate the sections chosen for comparison with the tip solutions.

recordings by applying the Beer-Lambert law $w = k \log_{10}(I_0/I)$, where $I_0$ and $I$ are the greyscale intensity values for a particular image pixel before and after a hydraulic fracture reaches that point and $k = 0.17$ mm is a calibration constant for the fracture fluid [9].

The following two experiments performed in the PMMA block with $\Delta\sigma = 4.3$ MPa are used for the purpose of comparison with the tip solution:

- positive stress jump experiment with fluid injection rate $Q = 0.0017$ mL/s, fluid viscosity $\mu = 30.2$ Pa s, $\sigma_{high} = 6.5$ MPa; and
- negative stress jump experiment with $Q = 0.0008$ mL/s, $\mu = 4.46$ Pa s, $\sigma_{high} = 7.52$ MPa.

## 4 COMPARISON BETWEEN THE TIP SOLUTION AND EXPERIMENTS

### *4.1 Positive Stress Jump*

Evolution of the penetration depth $\lambda$ is shown on Fig. 4a. The indicated value of the timescale $T$, (7), is determined by the fluid and solid properties and magnitude of the stress jump given in the previous Section, while the value of the crack tip velocity just prior to the crossing, $V_o$, is established by matching the experimental points with linear dependency $V_o t$. The evolution of the crack tip past the interface in the tip solution with constant $V_o$ agrees well with the experimental data up to penetration depths of about 10 mm. Comparison of the experimental fracture opening profiles (dots) with the tip solution using constant far field fluid velocity $V_o$ (dashed lines) is shown on Fig. 5. The eventual deviation of the tip solution from the experimental data is expected as the far field fluid velocity, set to the constant $V_o$ value in the tip solution, is bound to change (decrease) from this value in the

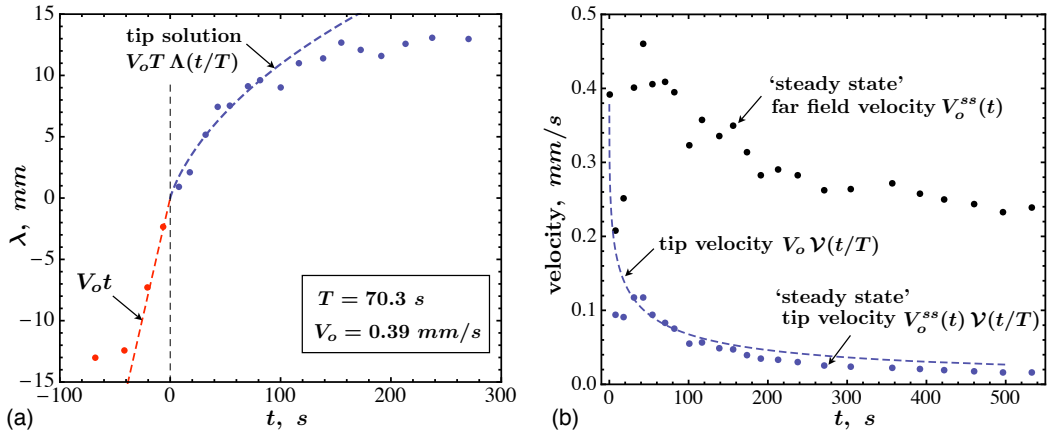


Figure 4: Positive stress jump: (a) Crack tip evolution; (b) Evolving 'steady state' far field fluid velocity $V_o^{ss}(t)$ and corresponding 'steady state' crack tip velocity $V^{ss}(t)$ in the tip solution. Dash line shows the tip velocity in the const. $V_o$ solution.

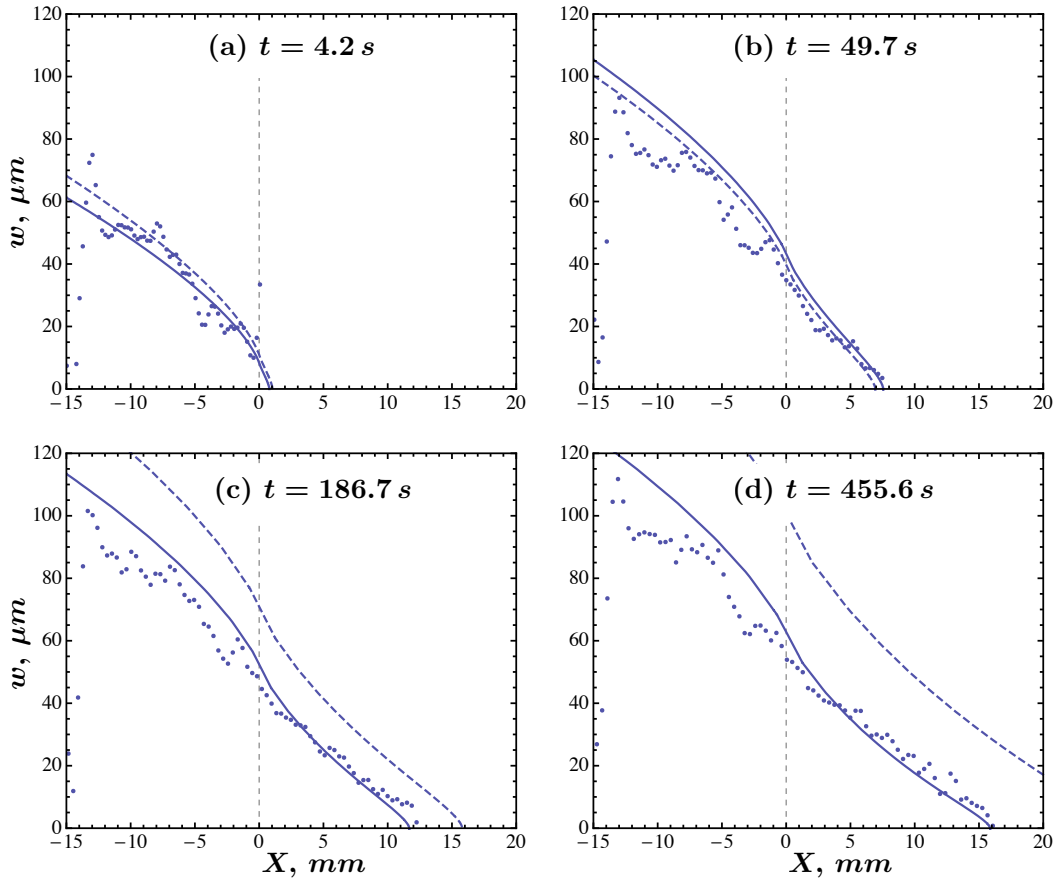


Figure 5: Positive stress jump: Comparison of experimental (dots) and the tip solution fracture opening profiles at various moments past the crossing. The tip solution corresponding to the constant value, $V_o$ , and evolving 'steady state' value, $V_o^{ss}(t)$, of the far field fluid velocity are shown by dashed and solid lines, respectively.

experiment. This change is underpinned by (i) partial redirection of the fluid flow along the interface (since fracture would tend to propagate more easily in that direction rather than into the high stress area across the interface, Fig. 3a); (ii) influence of the finite geometry of the experimental fracture that is not accounted for in the semi-infinite tip solution.

To improve the predictive capability of the tip solution, assume that the far field fluid velocity is evolving on a timescale smaller than the timescale that is intrinsic to the tip solution, $T$ (7). If this separation of timescales exists, then the tip solution, with $V_o$ equal to the instantaneous value of the time-dependent far field fluid velocity, can be regarded as a "steady state" approximation of the tip region. To find the steady state evolution of the far field fluid velocity in the tip solution, $V_o^{ss}(t)$, we simply equate the experimental penetration depth $\lambda^{\text{experiment}}(t)$ to the tip solution $(6_a)$-(7) evaluated at unknown $V_o = V_o^{ss}(t)$, i.e.

$$\lambda^{\text{experiment}}(t) = V_o^{ss}(t)\, T\, \Lambda(t/T) \tag{8}$$

Resulting $V_o^{ss}(t)$ and the corresponding steady state crack tip velocity, $V^{ss}(t) = V_o^{ss}(t)\, \mathcal{V}(t/T)$, are shown in Fig. 4b. Corresponding crack opening profiles, shown by solid lines on Fig. 5, agree very well with the experiment in practically entire penetration depth range.

### *4.2 Negative Stress Jump*

Similar to the earlier presentation of the results for the positive stress jump case, Fig. 6 shows (a) evolution of the penetration depth $\lambda$ in the negative stress jump experiment, contrasted to the tip solution (dashed line), for indicated values of $T$ and $V_o$; (b) the evolving steady state far field fluid velocity, (8), and corresponding crack tip velocity in the tip solution (dots), contrasted with the crack tip velocity in the tip solution when one takes a constant far field fluid velocity value $V_o$ (dashed line). The corresponding comparison of the crack opening profiles is shown in Fig. 7. The tip solution with the constant $V_o$ (dashed lines) agrees with the experimental

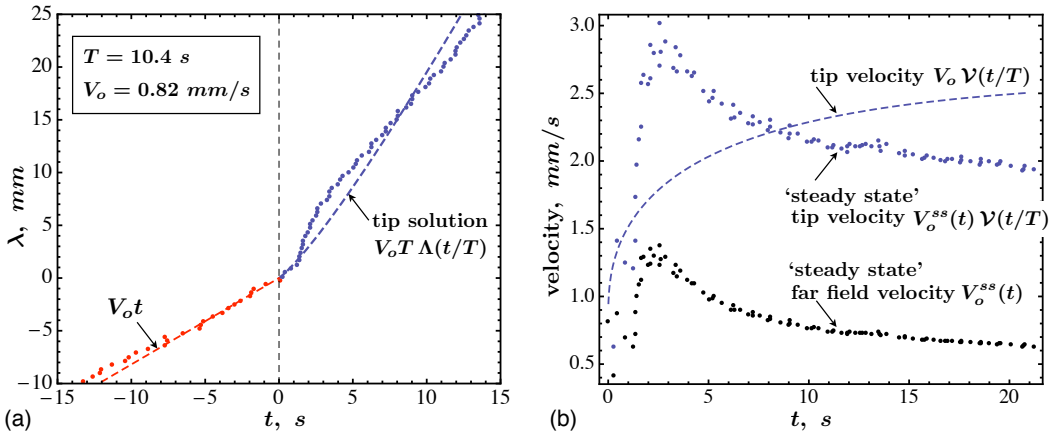


Figure 6: Negative stress jump: (a) Crack tip evolution, (b) $V_o^{ss}(t)$ and $V^{ss}(t)$.

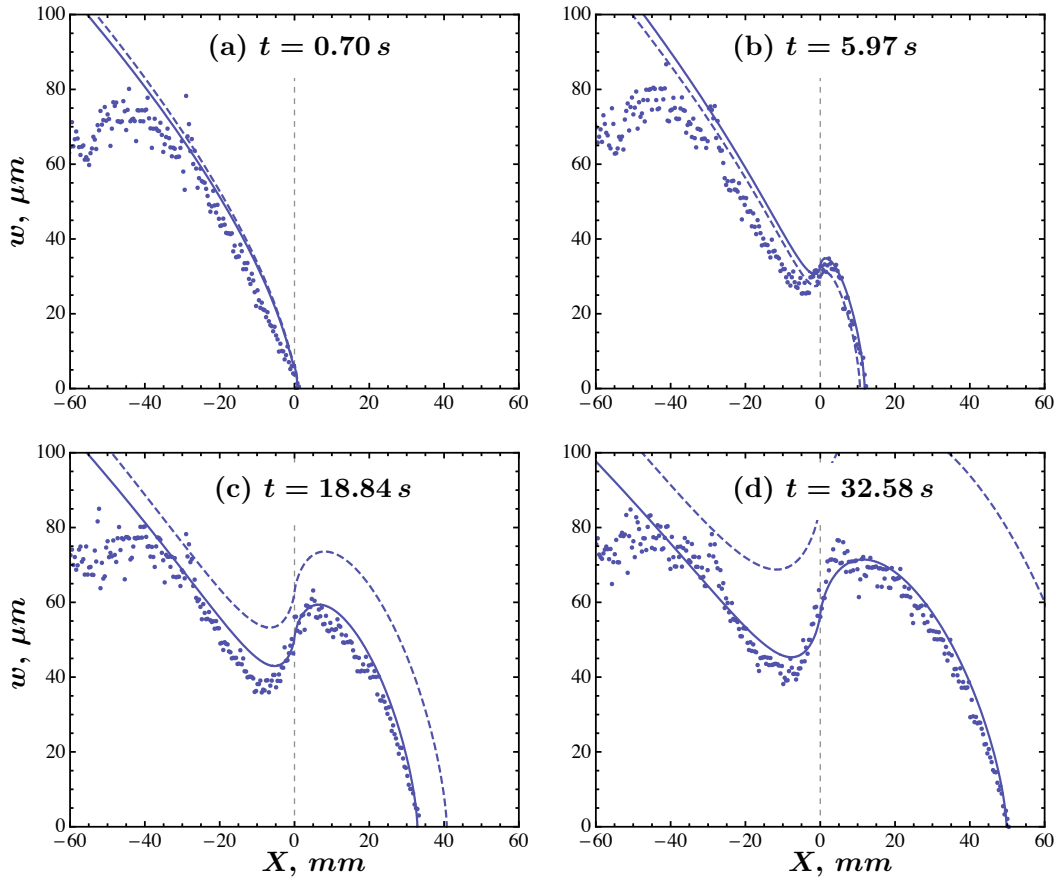


Figure 7: Negative stress jump: comparison of the experimental and theoretical crack opening profiles.

data only in very narrow (about 2 mm) initial penetration depth range. This state of affairs may indicate (among other possibilities) that (i) the far field fluid velocity for the tip region of the experimental fracture deviates (increases) very fast from the initial value $V_o$, owing to the rapid normal and *tangential* expansion of the fracture into the low stress (penetrated) side (Fig. 3b); and (ii) the existence of a non-negligible fluid lag. The fluid lag, which would not alter the transmission of light through the specimen, cannot be detected by the optical methods used here, leaving the check of the latter conjecture to future experimental and theoretical work. Nevertheless, the use of the steady state evolving far field fluid velocity in the tip solution, as detailed earlier for the positive stress jump case, allows for a good agreement of the theoretical (solid lines) and experimental crack opening profiles on Fig. 7 over nearly the entire experimental penetration depth range.

## 5 CONCLUSIONS

This paper compares the results from a theoretical solution of the tip region of a fluid-driven fracture crossing a stress interface with the experimental results for propagation of initially penny-shaped fractures across engineered stress jumps in

PMMA. The theoretical tip solution is limited in its original formulation to a small penetration depth range, where the fluid flow velocity into the tip region is approximately constant and equal to its value at the onset of crossing. This limitation is overcome by allowing the fluid flow velocity into the tip region to vary in the tip solution to reflect its changing nature in the experiment. Using this modified approach, the theoretical and experimental crack opening profiles are shown to be in close agreement throughout the entire measured range of penetration depths.

## 6 ACKNOWLEDGEMENTS

This work has been supported by Schlumberger (Integrated Productivity & Conveyance and Schlumberger Moscow Research) and CSIRO. Helpful discussions with E. Siebrits, A. Peirce, E. Detournay, and R. Jeffrey are gratefully acknowledged.

## REFERENCES

[1] D. I. Garagash. Scaling of physical processes in fluid-driven fracture: Perspective from the tip. In F. Borodich, editor, *IUTAM Symposium on Scaling in Solid Mechanics*, volume 10 of *IUTAM Bookseries*, pages 91–100. Springer, 2009.

[2] D. I. Garagash and E. Detournay. Plane-strain propagation of a fluid-driven fracture: Small toughness solution. *ASME J. Appl. Mech.*, 72(6):916–928, 2005.

[3] D. I. Garagash and E. Detournay. The tip region of a fluid-driven fracture in an elastic medium. *ASME J. Appl. Mech.*, 67(1):183–192, 2000.

[4] J. Desroches, E. Detournay, B. Lenoach, P. Papanastasiou, J. R. A. Pearson, M. Thiercelin, and A. H-D. Cheng. The crack tip region in hydraulic fracturing. *Proc. Roy. Soc. London*, Serie A(447):39–48, 1994.

[5] J. R. Lister. Buoyancy-driven fluid fracture: The effects of material toughness and of low-viscosity precursors. *J. Fluid Mech.*, 210:263–280, 1990.

[6] D. A. Spence and P. W. Sharp. Self-similar solution for elastohydrodynamic cavity flow. *Proc. Roy. Soc. London*, Ser. A(400):289–313, 1985.

[7] K. L. Johnson. *Contact Mechanics*. Cambridge University Press, 1994.

[8] R. G. Jeffrey and A. P. Bunger. A detailed comparison of experimental and numerical data on hydraulic fracture height growth through stress contrasts. *SPE Journal of Petroleum Technology*, 2007. Accepted for publication.

[9] A. P. Bunger. A photometry method for measuring the opening of fluid-filled fractures. *Meas. Sci. Technol.*, 17:3237–3244, 2006.